F. Benazzo, D. Rigamonti, P. Bettini, G. Sala, A.M. Grande
Interlaminar Fracture of Structural Fibre/epoxy Composites Integrating Damage Sensing and Healing
Composites Part B - Engineering, Vol. 244, 2022, 110137 (9 pages)
doi:10.1016/j.compositesb.2022.110137

Interlaminar fracture of structural fibre/epoxy composites integrating damage sensing and healing

F. Benazzo[1,2], D. Rigamonti[1], P. Bettini[1], G. Sala[1], A. M. Grande[1,*]
[1]*Department of Aerospace Science and Technology, Politecnico di Milano, Milano, Italy*
[2]*Aerospace Engineering, University of Michigan, Ann Arbor, MI*

*Corresponding author, antoniomattia.grande@polimi.it

Abstract

Technologies to control and reduce delamination damage in fibre reinforced polymer composites involve the use of fibre optic sensors and self-healing polymers, respectively. While the former technology can monitor the evolution of damage by measuring microscopic variations in the material's strain field, the latter can repair delamination damage by recreating broken interfaces. To evaluate the combination of these technologies, a high-performance epoxy vitrimer was used as the matrix phase of a fibre-glass composites incorporating Fibre Bragg Grating (FBG) sensors. Different laminates, manufactured with varying ratios a dynamic crosslinker and epoxy prepolymer, were compared. The analysis involved thermal characterization, mechanical tests to measure interlaminar fracture toughness, and microscope imaging of the cracked and repaired surfaces. Furthermore, FBG sensors to monitor in-situ damage and healing processes of the composites were employed. It was demonstrated that laminates with a larger proportion of dynamic crosslinker exhibit better repair abilities but lower thermal properties. The average and maximum recorded healing efficiency at the first healing cycle, calculated based on the critical fracture toughness, were at 89% and 95% respectively, while it averaged a steady 50% efficiency after several repairing cycles.

1. Introduction

In the aerospace industry, structures not only need to be resistant to the stresses applied, but also be light enough to satisfy the weight limits of the whole system [1]. The need for sufficiently strong and comparatively light materials is generally met in the aerospace sector by composite materials, which provide great strength in many directions and are adaptable to almost any environment. Depending on the application, the combination of matrix and reinforcement phase can indeed be varied with ease. Despite these advantages, composites can be very weak under specific types of stresses.

Delamination is a failure mode for composites that involves the separation of layers from each other [2]. If an interlaminar crack forms, it can propagate throughout the whole composite, causing catastrophic failure. A novel approach to repair delamination damage includes the use of self-healing polymers as matrix phase, which encompass several types of healable materials characterised by varying repair strategies [3]. Yet, the common feature is the ability of these materials to repair existing damage or cracks autonomously or under specific environmental conditions, and thus restore mechanical and functional properties.

Self-healing and healable materials can be classified in two main categories, extrinsic and intrinsic [4,5]. Extrinsic approaches involve the use of micro-capsules or microscopic hollow tubes [6], which rapture during the damage event and thus cause the in-situ release of the healing agent. Microvascular networks have the benefit of being connected to a reservoir of healing agent, meaning that the latter can be supplied continuously in the site of damage. Nonetheless, the integration of this extraneous network of vessels in the matrix can determine several stress-concentration points that hinder the mechanical properties of the composite. On the other hand, intrinsic healing approaches can exploit either shape memory effects [7–9] and reversible bonds [10–12] to close the crack and restore interfacial properties, respectively. For example, Zhang et al. [13] presented how a cyanurate-oxazolidone based matrix can be implemented in a carbon-fibre composite to produce a material that healed interlaminar damage. Healing was a result of the cleavage of isocyanurate

groups during mechanical testing, which would then transform into oxazolidone rings through thermal stimulus. The study demonstrated that intrinsic healing matrices could allow for the restoration of up to 85% of the interlaminar shear strength and, most crucially, can be implemented in a composite material with stiffness and thermal performance comparable to current aerospace grade composites. Post et al. [14] also investigated intrinsically healed matrices, adopting a repairable thermosetting matrix based on Bis [3-(triethoxysilyl)propyl]disulfide. The investigation observed that mode I fracture, and impact damage can be healed multiple times with the sole use of pressure at the site of damage. These studies lead to the conclusion that composites made from self-healing or healable matrices with reversible bonds have the potential to be employed in structural composites including mechanical properties comparable with traditional materials, improved long term performance and damage management ability thanks to the self-repair functionality.

To properly evaluate the resistance to delamination of a composite, the material property that is most appropriate is interlaminar fracture toughness (G) [6], which is the ability of a composite to resist to the propagation of cracks that generate between layers, *i.e.* delamination. There are three modes of interlaminar fracture, each with a set of mechanical tests that may be employed to quantify the resistance to delamination. Mode I, which involves the separation of layers by opposite pulling of two halves of the composite, is generally tested through double cantilever beam (DCB) tests; mode II involves the sliding of adjacent layers on top of each other and is measured with different end notch flexure (ENF) tests; mode III is instead the lateral sliding of layers and is rarely measured due to the complexity in the testing apparatus. Kostopoulos et al. [15] made use of both mode I and II tests [15] for the investigation of the healing ability of nylon microparticles doped with carbon nanotubes. The 3-ENF tests provided easily identifiable critical loads indicating the specimens' fracture, but only the DCB tests provided information about the interlaminar propagation of the crack. DCB mechanical tests have also been employed in the large majority of investigations concerning mendable composites, but, in the prospect of aerospace applications, mode II fracture should draw equal attention from the scientific community. Principal loading modes in aircraft structures, such as fuselage pressurization and material thermal gradients, involve mode II interlaminar stresses that may be repaired through healing matrices. For these reasons, 4-point ENF testing, greatly similar to 3-ENF but characterised by a steady crack propagation due to the larger specimen area under flexural stress [16–18] is a suitable method for investigations with such novel composite materials. ENF mechanical tests consider an energy approach to determine the resistance to interlaminar crack propagation, while a more direct approach to measure the resistance to delamination may be taken through short beam shear (SBS) testing. This test measures the strength required to cause the material to fail under a 3-point bending loading and it is considered to study mechanical properties after a healing cycle. Notably, it was employed by Heo and Sodano [19] in the characterization of a healable polyurethane.

In all these testing methods, crack propagation and matrix healing are interlaminar processes and, as a result, visually monitoring their behaviour may be very challenging. Several structural health monitoring technologies that have been developed for this application, namely piezoresistive sensors, acoustic emissions sensors, and comparative vacuum monitoring [20], are characterised by numerous shortcomings. These include the introduction of films between the composite layers, which can inhibit the composite mechanical properties, or the challenges inherent to the data from these sensors, which may not easily point to the presence and nature of the damage. Contrarywise, optical fibres offer a less intrusive and more promising approach that has already been employed to monitor composite's crack propagation successfully [21,22]. In particular, the integrations of these glass fibres along with Fibre Bragg Grating (FBG) sensors [23] have also been employed to monitor a series of phenomena that are unique to fibre composites. For example, the erratic behaviour of unidirectional laminates under fibre bridging was thoroughly compared and investigated through multiple carbon fibre specimens implemented with FBG sensors [24,25]. Similarly, the correct curing of a composite material was examined by looking at the strain generated during the cross-linking of the matrix phase [26]. More crucially, these sensors can be adopted in a healable composite to monitor the interlaminar stress field during the healing cycle, in a manner that has never been previously explored so far.

This investigation looks at the healing efficiency of a dynamic covalent based epoxy vitrimer previously investigated in other studies [27–29], and consisting of diglycidyl ether of bisphenol-A epoxy (DGEBA) as

prepolymer and 4-aminophenyl disulphide (4-AFD) as hardener. Vitrimers are unique in their versatility, which results from material properties simultaneously similar to both thermosetting and thermoplastic polymers. These properties resulted in the ability of these materials to be employed for a range of applications, such as shape memory polymers [30], matrices to align infused microfibres [31], and matrices capable of repairing the fibre-matrix interface in CFRPs [32]. In this study, the epoxy was used as matrix phase with fibre-glass fabrics as reinforcement and FBGs as in-situ sensors to manufacture multifunctional composites. Composites samples were then tested through 4-ENF mechanical tests at varying hardener concentrations to observe how these affect the healing efficiencies, while SBS tests were employed to confirm that resistance to layer debonding was achieved. Furthermore, the implementation of the fibre optic analysis during these tests and the healing cycle allowed to understand the behaviour of internal stresses during the healing process and how an autonomous damage and delamination sensing system could be integrated. Such insights on the internal stresses during healing had never been explored before and offer more details on the stresses through the composite post-damage.

Composite materials that include either self-healing polymers or fibre optics fall into the category of smart materials, the implementation of both into one single composite laminate, illustrates one approach to create a complex aerospace structure, consisting of multifunctional components. This leads the engineering community one step closer towards a complete smart structure that can accurately mimic all human biological processes. Furthermore, the mendable composite coupled with the optical fibre architecture could offer a viable alternative to airframe maintenance, which is currently expensive, involves the creation of a discontinuity in the composite structure, and determines an increase in total weight.

2. Experimental methods

2.1. Materials

The self-healing composite investigated in this research consisted of a glass fibre reinforcement phase and a dynamic covalent epoxy vitrimer matrix. Glass fibre twill 2/2 fabrics (Hexcel HexForce® 01102) with a nominal weight of 290 g/m² were cut into 80x150mm rectangles prior to lamination. Three sets of epoxy matrix were produced using diglycidyl ether of bisphenol-A epoxy (DGEBA, Sigma-Aldrich) as prepolymer. Two dynamic epoxy based vitrimers with healing ability were synthesized using 4-aminophenyl disulphide (4-AFD, >95%, Sigma-Aldrich) as hardener, while the second epoxy resin used as non-healing reference was obtained substituting 4-AFD with 4,4′-ethylenedianiline (>95%, Sigma-Aldrich).

The optical fibre system consisted of an array of two sensors (FBGS manufacturer) with nominal Bragg wavelength 1547 and 1565 nm. The gauge length was 8 mm and the distance between sensors 50 mm. FBGs were inscribed in a single mode fibre with 80 μm cladding diameter, and Ormocer-T coating for heat resistance. The signal was acquired through a SM130 Optical Sensing Interrogator equipped with the Micron Optics ENLIGHT software for the identification of the peaks.

2.2.Composite manufacturing

The manufacturing of the composite consisted in a wet layup of 20 glass fabric layers in an aluminium mould that measured 80x150mm, shown in Figure 1. The average thickness of the specimens was 4.7± 0.1 mm, including a PTFE film (10 μm thickness) as crack initiator after the 10^{th} layer.

In total, three epoxy mixtures were used: the stoichiometric mixture (36.5g of 4-AFD for 100g of DGEBA), the non-stoichiometric mixture with an excess of hardener (43.8 of 4-AFD for 100g of DGEBA), and the reference mixture (31.2g of 4,4′-ethylenedianilineis for 100g of DGEBA). The ratios of the stoichiometric and reference mixtures were calculated to obtain a 1:1 ratio between the amine bonding groups in the hardener and prepolymer, while the non-stoichiometric mixture followed the same ratio as described by Luzuriaga et al. [27] which involved a 20% increment of the hardener. For all epoxy matrices, the two components were slowly mixed in a beaker on a heated plate at 80°C and later degassed for 20 min. The glass fibre layers, and epoxy were laid up by hand and the final laminate was cured in a hot press. This involved placing the laminate in a vacuum bag and under 2.5 bars of additional pressure at 120 °C for 120 minutes for initial curing and then at

150 °C for 120 minutes for post-curing. In total three 20x150mm specimens were cut from each of the laminates produced. An additional laminate, consisting of the non-stoichiometric mixture, was cut to obtain 6 identical 20x40 mm specimens for SBS testing.

The specimens that included the FBG sensors were manufactured with the same method, except for the placement of the optical fibres with FBG sensors between the 8th and 9th fabric layers. Protective sheaths were used in proximity of the mould holes to avoid that the pressure exerted on the laminate and the sharp edges of the holes would damage the fibres. The optical fibre was placed such that the sensors were aligned with the 4-point bending apparatus, as shown in Figure 2.

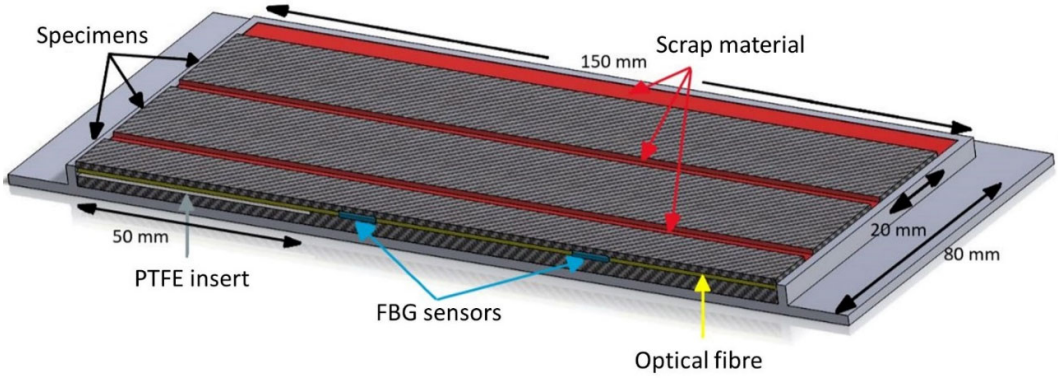

Figure 1: Representation of the mould and laminate, with the difference components and their placement.

2.3. Thermal analysis

For the three epoxy matrices, a differential scanning calorimetry (DSC) analysis was employed to determine the materials' thermal behaviours. To test that the epoxy in the specimens had the proper curing cycle, the glass transition temperature (T_g) of the substance were measured after composite manufacturing. DSC analysis was also employed to provide insight on the epoxy's T_g variation after the healing processes.

2.4. Mechanical testing

The mechanical test adopted to evaluate the interlaminar fracture toughness was the 4-ENF test. A MTS testing system (Model 858) equipped with a 15 kN load cell was employed for the fracture experiments. A sketch of specimen positioning for the mechanical test are shown in Figure 2. Crosshead speed was set to 1 mm/min. All experiments were performed at room temperature.

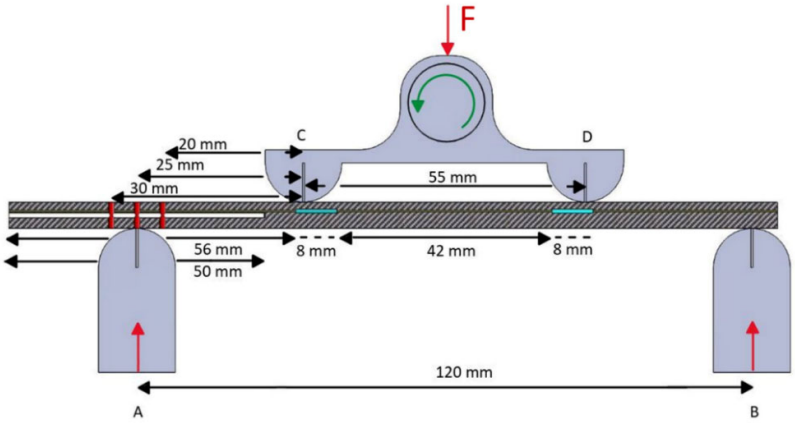

Figure 2: 4-ENF apparatus with loading noes dimensions, specimen position, and location of the PTFE insert and FBG sensors in the testing apparatus.

Calibrations to obtain the compliance were performed at 20 and 30 mm between the PTFE insert and the left loading nose, and full fracture tests at 25 mm. To create the R-curve of the propagation of the crack, the test was recorded with a camera. Each specimen was not only tested after the healing cycles, but also once before the first healing process to provide a reference load-displacement curve for non-repaired and cracked specimens. The data reduction of the test method employed is consistent with 3-ENF testing (ASTM D7905), however, as shown by Pérez-Galmés et al. [16] and Oliveira et al. [17], the relationship between compliance and crack length is linear, and, ultimately, the formula for the mode II interlaminar fracture toughness ($G_{II\,C}$) becomes:

$$G_{II\,C} = \frac{P^2}{2B} * C_1 \tag{1}$$

where B is the specimen's width, C_1 is the parameter from the compliance calibration, and P is the critical load. In the case of this investigation, P was the load measured at the first non-linear point on the load-displacement curve, which coincided with the crack's propagation. The equation was similarly used to create R-curves for the virgin and repaired specimens by changing the load P with the load at the current crack length and calculating C_1 as the reciprocal of the gradient of the load-displacement curve again at the current crack length. Finally, to investigate the relationship between the crack interface and the healing process, the cracks of the virgin and healed specimens were photographed and compared with 80x magnification at an optical microscope.

The SBS tests, employed to confirm the results of 4-ENF testing by measuring the healing efficiency of the interlaminar shear strength (ILSS) of the specimens, was performed as presented in the ASTM standard D2344. This involved using shorter specimen than in 4-ENF tests and set them in a 3-point fixture that, thanks to the large height to length ratio of the specimens would promote shear between the layers rather than bending stress. To analyse the data, equation (2) below was employed:

$$F_{SBS} = 0.75 * \frac{P_m}{b * h} \tag{2}$$

where the maximum load P_m, the width b and thickness h of the specimen provide the resistance to shear (F_{SBS}).

2.5. Self-Healing Process and Healing Efficiency

To activate the healing behaviour of the epoxy vitrimers with the dynamic disulphide bonds, the specimens were placed in a heated press at 200 °C under 100 bars of pressure for 10 minutes. The healing efficiency was calculated using equations (3) and (4) for mode II fracture toughness and ILSS, respectively, where $(property)_i$ represents the value in the bracket calculated after the i^{th} healing cycle and $(property)_{virgin}$ represents the value in the bracket calculated before any healing took place and the specimen was uncracked.

$$Healing\ Efficiency_{G_{II\,C}} = \frac{(G_{II\,C})_i}{(G_{II\,C})_{virgin}} * 100 \tag{3}$$

$$Healing\ Efficiency_{F_{sbs}} = \frac{(F_{sbs})_i}{(F_{sbs})_{virgin}} * 100 \tag{4}$$

2.6. FBG integration

Mechanical and thermal considerations were made when selecting the optical fibre, following evidence from previous studies [33]. Due to the negative influence on mechanical properties that the inclusion of a fibre in composites may have, the cladding diameter of the chosen fibre was reduced to 80 µm. In addition, since the composite curing and healing necessitated high temperatures, the selected fibre coating was the Ormocer-T coating, which resits temperatures well above the 200 °C. Similar care was used for the placement of the FBG sensors in the fibre. The first sensor was placed 6 mm from the PTFE insert to ensure that during the 4-ENF test the two sensors would be symmetrically placed with respect to the loading noses of the apparatus, as shown in Figure 2. This allowed for even bending of the two sensors, and thus permitted a fair comparison of the data

from the sensors to evaluate the advancement of the crack. The sensor closest to the PTFE insert and that closest to the tail of the specimen will be regarded from now on as the crack and tail sensors respectively.

One noteworthy phenomenon observed during the optical fibres data analysis is peak splitting, which involves the distortion of the signal [34,35]. The onset of peak splitting may indicate peculiar strain fields around the optical fibre sensor; however, the current investigation aims at observing the simple bending of the sensors during the 4-ENF test and monitoring the internal stresses during the healing process at a fundamental level due to the novelty of the approach. As a result, the analysis of the spectra obtained from the FBG sensors involved fitting a gaussian curve to the processed signal, following the wavelength variation of the spectral peak, ultimately averaging the signal, and disregarding any splitting behaviour. By comparing these results to the healing efficiencies from fracture tests, correlations could be drawn between the quality of the healing process and the sensors' response, leading to a non-invasive method to assess healing.

3. Results and discussion

The repair capabilities of the fibre-matrix combination adopted had to be evaluated and compared to the reference matrix phase. This was carried out through the 4-ENF tests of laminates manufactured with the three matrices. During the tests, recordings of the crack's propagation along with load-displacement plots (Figure 3), permitted the creation of R-curves of the material at different stages of healing (Figure 4). The data as then summarized and listed in Table 1, which clearly shows that proper and continuous healing only occurs in the non-stoichiometric mixture specimens. As expected, the reference mixture did not repair the interlaminar cracks, but a substantial difference between the stoichiometric and non-stoichiometric vitrimers was observed. Healing can be attributed to the chemical re-shuffling of disulphide bonds during the healing process, as investigated in previous studies [24, 25, 28]. Since healing requires the proximity of the dynamic bonds to reverse the cleavage of the latter during testing, it is statistically more likely for the reaction to take place if a higher concentration of hardener is present, as in the non-stoichiometric mixture.

Table 1: Average fracture toughness and healing efficiencies for 4-ENF tests.

Matrix	Healing cycle [-]	$G_{II\,C}$ [J/m^2]	Healing efficiency [%]
Non-stoichiometric	Virgin	1688 ± 85	-
	1	1496 ± 196	88.6 ± 11.6
	10	847.6 ± 29.1	50.2 ± 1.7
Stoichiometric	Virgin	1213 ± 239	-
	1	483.5 ± 203.2	40.0 ± 16.8
	2	162.7 ± 28.5	13.7 ± 2.4
Reference	Virgin	766.0 ± 296.4	-
	1	No healing	

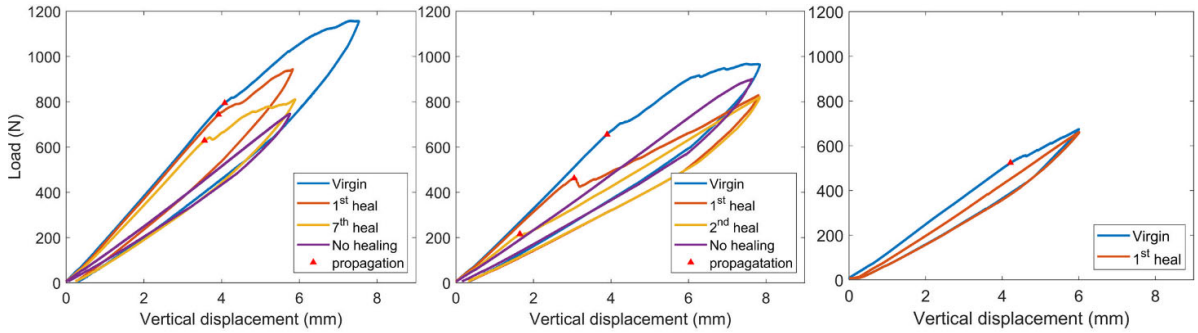

(a) (b) (c)

Figure 3: Representative load-displacement curves for the three different composites: (a) non-stoichiometric mixture specimen, (b) stoichiometric mixture specimen, and (c) reference mixture laminate. The red triangles represent the data points where the curves cease to be linear, and the crack starts to propagate. The reference laminate's 1st heal curve is coincident with its no heal curve as the specimens did not show any form of mending ability.

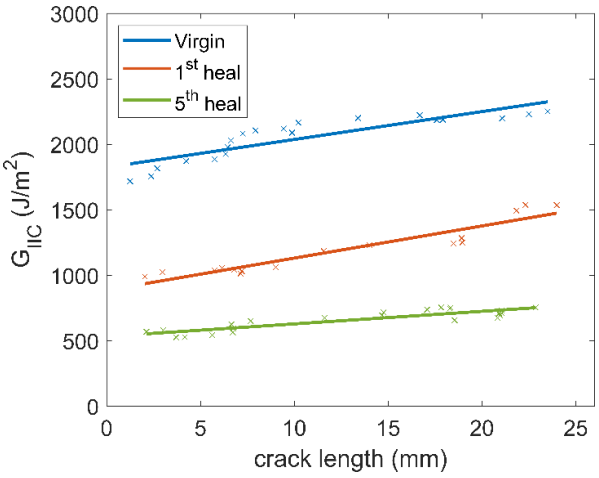

Figure 4: R-curves at different healing cycles during 4-ENF testing.

As the mixture with proper healing was identified, further analysis was conducted on the non-stoichiometric specimens to observe the healing process from several perspectives, namely mechanical performance, thermal analysis, optical surface examination, and internal stress analysis through optical fibres' sensors. First, the recovery of fracture toughness was evaluated by 10 cycles of 4-ENF tests of all the non-stoichiometric specimens. The resulting healing efficiencies (Figure 5), display an initial average repair of about 89% fracture toughness, and a steady 50% recovery even at the 10th healing cycle. The excess of hardener is definitely contributing to the recovery of fracture properties, but its effects is reducing with healing cycles reaching a healing efficiency value close to the one of the stoichiometric matrix after the first healing cycle.

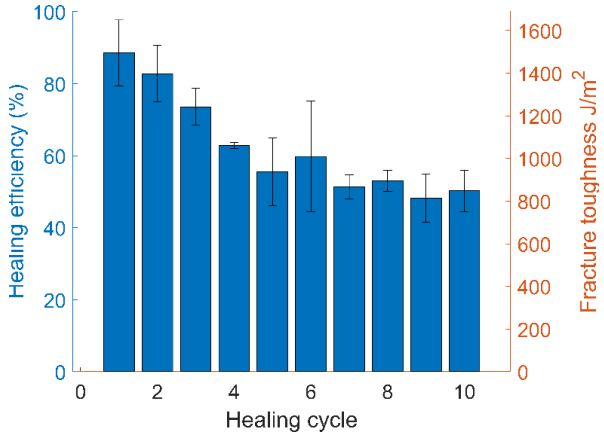

Figure 5: Efficiency after each healing cycle for the non-stoichiometric specimens

SBS tests confirmed the trend of decreased healing with increasing healing cycles. As shown in Figure 6, there is a steady decrease in the recovery of ILSS as the healing cycles progress, which does not necessarily mean that the healing did not take place as un-repaired specimens would provide no resistance to the load until a new crack is formed. As presented by the load-displacement curves between the 1st and 3rd healing cycles, the plots are considerably similar, providing evidence for an almost constant level of damage repair. Yet, the steady drop in efficiency is attributed to the partially plastic failure mode of the specimens. In these tests, the lack of a crack initiator that guides the crack development between the middle layers allows for the fracture to

grow along the vertical loading plane, damaging the reinforcement as well as the matrix phase. Even though the tests were stopped as soon as a drop in load was observed, the partial damage of the fibres may not be avoided and, more importantly, cannot be repaired. Despite the effects of this unwanted failure mode, it appears that the healing process restores ILSS as well as fracture toughness.

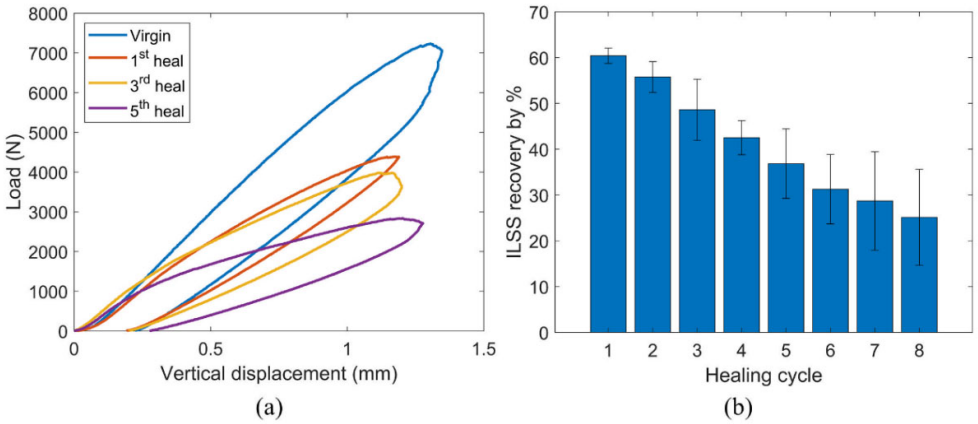

Figure 6: SBS fracture tests: (a) load against vertical displacement for different healing cycles, (b) the healing efficiency as a percentage change in ILSS, calculated for up to 8 healing cycles.

To substantiate the healing through a re-shuffling of the disulphide bonds, thermal analysis by DSC tests was carried out. The data obtained (Table 2) provided the T_g of the epoxy before and after several healing cycles at 200°C showing that the laminates were fully cross-linked after the curing process. In addition, the results indicate that there were no changes to the cross-linking chemical bonds during healing, as the T_g remained unvaried. However, different T_gs were observed for the non-stoichiometric and stoichiometric. In details, the former has a lower T_g, potentially indicating a plasticising effect (higher network mobility) of the excess the hardener and reflecting the higher fracture toughness measured for the virgin material.

Table 2: DSC measured T_g for the three matrices after the curing cycles and after the healing cycles.

Matrix	**T_g after curing [°C]**	**T_g after 5th healing cycles [°C]**
Non-stoichiometric	159.0	158.0
Stoichiometric	173.8	172.3
Reference	183.6	185.0

The optical surface investigation indicated a preferred path of propagation for the crack. Enlargements of the surface of virgin and cracked specimens, shown in Figure 7, primarily demonstrates that the crack was repaired successfully on the surface of the specimen. More notably for the current observation, the images display 'landmarks' of the cracks that can be seen in both the virgin and repaired specimens. Examples of these landmarks, which include large resin deposits or imperfections, can be seen at the centre of the crack of the top and bottom pictures. This aspect prove that the first crack propagation is a preferred path for subsequent faults to develop along. Thus, even though the dynamic bonds have been re-established, the other molecular bonds that were broken in the mechanical tests caused a slight reduction in the resistance to crack propagation. Finally, the first and second images show edges of the crack in the virgin specimen that are not as smooth as those in the repaired specimen. This can be attributed to the fact that during the healing process the polymer network gain mobility and the large pressure forces the resin to be redistributed to possible fill some of the gaps that formed in the curing cycles and smooth the cracked surfaces generated during fracture.

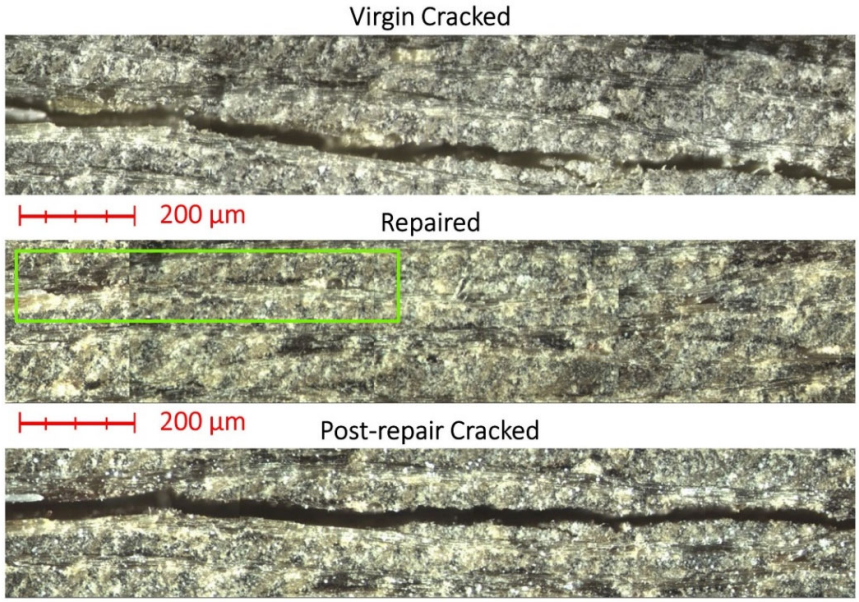

Figure 7: Pictures with 80x enlargements of the same specimen at three different testing stages. The green area represents the region where the crack was healed.

To evaluate crack evolution, a comparison between the resistance to crack propagation between virgin and repaired specimens was performed through the R-curves of the 4-ENF tests in Figure 4. These clearly display an initial G_{II} for the virgin that is considerably larger than that of the healed specimens, thus conforming to the results observed when comparing the critical G_{II} of the various tests. Furthermore, there is a general trend of diminishing gradient of the lines as the number of healing cycles increases. The positive gradient of R-curves in 4-ENF tests has been studied extensively [27-29] and attributed to both the manner in which the specimens are loaded and interlaminar fibre bridging. Since fibre bridging is not common but still a plausible phenomenon in woven composites [40], and since it is extremely difficult to notice in mode II mechanical test due to the closed interlaminar interface, it is more likely that the high rotation at the pins has caused the upward slope of the curves, while the diminishing gradient coincides with the decreasing fracture toughness between healing cycles.

To gain insights on the internal stresses and process that occurred between the composite layers during testing, the data from fibre optic sensors was analysed by associating any change in wavelength to a strain, according to:

$$\Delta\lambda_b = \lambda_b(1 + p_e)\varepsilon \tag{5}$$

where p_e and ξ are the photoelastic and thermo-optical constants, and ε is the measured strain.

The correct functioning of the sensors was validated by comparing the strain in the tail sensor with the load on the specimen (Figure 8). The two curves are identical, although the strain is negative, indicating a compressive strain since the sensor was above the mid-line of the composite during the bending of the specimen. When the crack sensor is considered (Figure 9), the plots of the two sensors diverge at 300 seconds: the tail sensor continues to be under compression, while the crack sensor displays a peak in strain, up to approximately 10.000 micro-strains. This is substantiated by the load-time plot in Figure 8, which becomes non-linear at 300 seconds, indicating the propagation of the crack, but can also be clearly attributed to the crack being sensed by the crack sensor and the consequent variation to the stress field around it. The propagation of the crack causes the specimen to separate into two equal laminates: the top half housing the optical fibre and the bottom one. In the top half, the optical fibre is now on the bottom of the mid-line and, as the layers of the composite are freed from the constraint of the bottom half, the bent section acts as a beam under bending stress. Thus, the fibre is

no longer under compressive stress, but increasingly more under tensile stress. This corresponds to the positive value of the strain observed by the crack sensors alone.

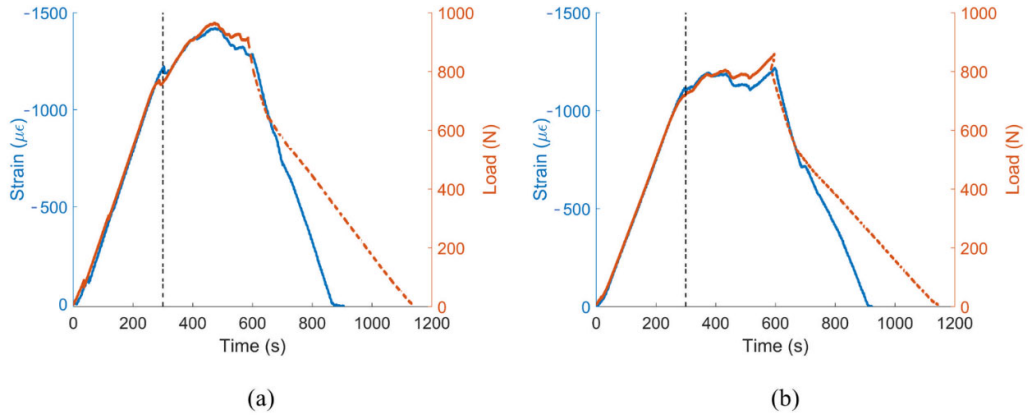

Figure 8: Strain calculated from the crack sensor data for the (a) virgin specimen and (b) repaired specimen, compared to the loads measured during the fracture test. The dashed lines indicate the unloading of the specimen, which occurred at faster crosshead speeds.

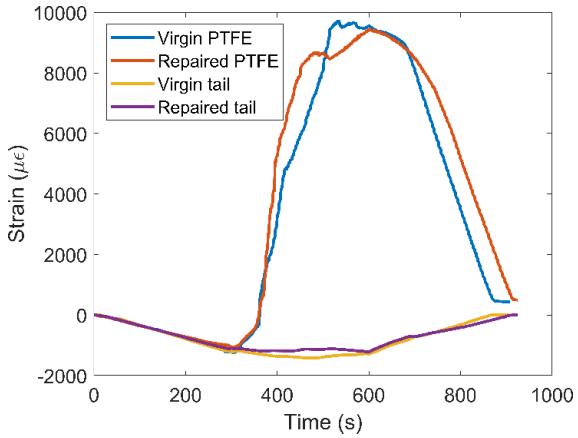

Figure 9: Strain as a function of time calculated from the two FBG sensors in both the virgin specimen and once repaired 4-ENF test. The loading of the specimen id terminated at 600 seconds, when unloading begins.

The virgin and repaired plots presented were obtained from a specimen that displayed 95% first healing efficiency, only approximately 6% off the average value from Table 1, yet still within one standard deviation from the value. Therefore, comparisons between the sensors' data during the mechanical tests could provide significant information on the data that well-repaired specimens exhibit. The first distinctions between the virgin and repaired fractures can be drawn by observing the strain and load curves as a function of crack length (Figure 10), where the crack sensor identified the propagation of the damage from a farther distance in the repaired specimen than in the virgin one. The strain curve in the repaired specimen is approximately 3 mm farther to the left than the virgin specimen's curve, demonstrating that the strain on the sensor was different for the two tests, despite the crack having propagated an equal amount. This is strictly linked to the process zone of the FBG senor, which constitutes the area in which a damage formation can be identified in the data from the sensor. In the healed interface the network of polymer chains has been damaged and the links between them have been only partially re-built and re-organized in the healing cycle. This has made the material more susceptible to damage formation, determining a larger process zone than in the virgin specimen. The load and strain curves of the virgin sample also present large jumps at 12, 15 and 17 mm that demonstrate the discrete increments in the length of the crack. Instead, the healed sample had a more continuous crack propagation. This difference in growth propagation can be explained by the images in Figure 7 that demonstrates how the pressure and heat applied in the healing process compact the resin leading to a less brittle fracture, ultimately

improving interlaminar resin distribution. Therefore, there are less defects, voids, lumps of resin that may cause these discrete jumps. These also indicates one of the many advantages of the implementation of optical fibres, which allow to predict the state of the laminate and provide warning to prevent catastrophic failure.

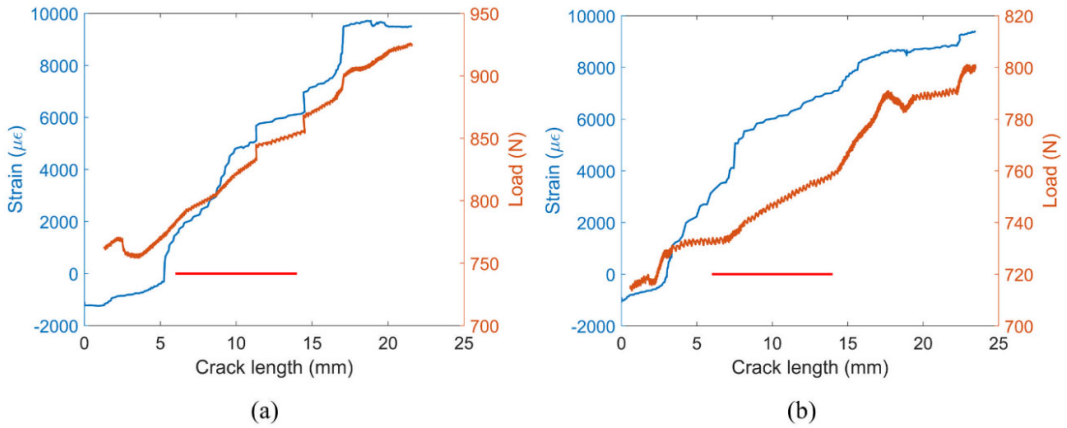

Figure 10: Strain and load as functions of crack length for the two tests: a) virgin specimen and b) once repaired specimen. The red lines in both plots represent where the crack FBG sensor was placed along the crack's path.

Provided the high degree of healing efficiency of the specimen with optical fibres, the inclusion of FBG sensors allowed to correlate the high degree of healing of the matrix phase with the signal from an FBG sensor in a section of the composite under repair, *i.e.,* the crack sensor. The data from the tail sensor was instead used as reference as no healing took place in the undamaged tail section. This evaluation, represented in Figure 11, shows the wavelength measured by the two FBG sensors during the healing cycle, and clearly exhibits an initial steady rise in wavelength as a function of time due to the heating of the specimens. However, as expected, the two sensors then diverge since the crack sensor was in the damaged zone and the matrix underwent healing, while the tail sensor was simply heated and cooled. The tail sensor indeed shows a flattening curve as the temperature controller attempted to reach 200 °C, followed by a constant 10-minute interval as per healing cycle, concluded by the cooling of the specimen. The crack sensor instead displays a maximum wavelength at 35 minutes, and surface temperature of 180 °C. This could be a sign of the starting of healing, corresponding to the closing of the damaged interface. This closing action further constrain the sensor, which would, in turn, respond by decreasing the peak wavelength, as observed during the compression of the fracture tests.

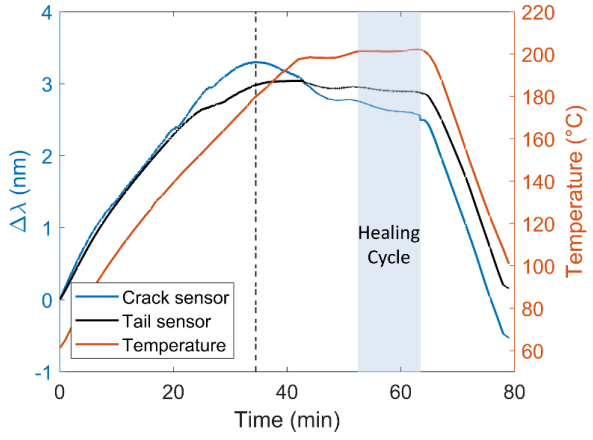

Figure 11: Peak wavelength of the crack and tail sensors during the healing process. The vertical lines show what the surface temperature of the specimen (measured by a thermocouple) was at certain points during the healing. At the start of the test the temperature reading was 60°C and raised up to 200°C, at which point it was kept constant until 70 minutes (total time at 200 °C equal to 10 minutes), when the cooling process began.

Nonetheless, a full analysis of the strain on the sensor during healing requires information about the internal temperature of specimen. In this case, the employment of a thermocouple measuring only the surface temperature limits the observations that can be drawn from the experiment.

4. Conclusions

Among the several types of self-healing and healable materials, dynamic covalent bonds-based polymers offer great potential. The epoxy matrix employed in this research has been proven to heal thanks to the dynamic disulphides, and the concentration of dynamic moieties was found to have a clear effect on the repair capabilities. Fracture tests of the non-stoichiometric mixture composite have shown an average fracture toughness recovery of 89% after the first fracture cycle and a constant 50% repair in the long-term, despite a decrease in T_g compared to stoichiometric and reference matrices. Microscope imagining also proved that the first healing process helps to reduce the percentage of voids in the material and repairs the cracked interface. However, the same images also prove that the path of the first crack is a preferred route for future cracks. This demonstrates that only a fraction of the bonds has reformed, which supports the partial restoration in interlaminar fracture toughness. Finally, SBS tests showed evident differences between healed and non-healed specimens, demonstrating that also shear strength is restored in the composite. However, the fracture mode of the specimens caused damage in the matrix-phase as well as the reinforcement phase, which could not be repaired by the healing cycle, thus indicating the not complete appropriateness of this test procedure to evaluate healing performances.

The inclusion of FBG sensors demonstrated the damage sensing functionality of the composite and provided additional information about the differences between virgin and repaired specimens. The comparison between the data from the crack and tail sensor, along with the load curves, proved the correct functioning of the optical fibres and the ability of the sensors to monitor the crack, all without hindering the healing ability of the mendable matrix phase. In addition, it was shown that the process zone of the sensor was wider in the repaired specimen and that the crack propagation was faster in the repaired material.

Future developments of this investigation could involve refinements to the FBG sensors system to improve its sensitivity and correlate the material damage/repair status to the monitoring system data, as well as the implementation of this healable laminate into aerospace applications. Since the foremost objective of this study is to provide an alternative solution to the currently available options to composite maintenance in the aerospace industry, the use of welding technologies on the damaged area of the composite could be investigated as possible way to thermally activate and to promote local healing.

Acknowledgements

The authors want to acknowledge the Italian Space Agency (ASI) for the support. Grant agreement 2018-5-HH.0.

References

[1] Dry C. Self-repairing composites for airplane components. Sens. Smart Struct. Technol. Civ. Mech. Aerosp. Syst. 2008, vol. 6932, International Society for Optics and Photonics; 2008, p. 693212. https://doi.org/10.1117/12.776497.

[2] Tessema A, Ravindran S, Kidane A. Damage Evolution and Local Strain Redistribution in Composite Laminate with Various Fiber Arrangements: Proceedings of the 2018 Annual Conference on Experimental and Applied Mechanics. Conf. Proc. Soc. Exp. Mech. Ser., 2019, p. 97–102. https://doi.org/10.1007/978-3-319-95879-8_16.

[3] Zhang P, Li G. Advances in healing-on-demand polymers and polymer composites. Prog Polym Sci 2016;57:32–63. https://doi.org/10.1016/j.progpolymsci.2015.11.005.

[4] van der Zwaag S, Grande AM, Post W, Garcia SJ, Bor TC. Review of current strategies to induce self-healing behaviour in fibre reinforced polymer based composites. Mater Sci Technol 2014;30:1633–41. https://doi.org/10.1179/1743284714Y.0000000624.

[5] Paolillo S, Bose RK, Santana MH, Grande AM. Intrinsic Self-Healing Epoxies in Polymer Matrix Composites (PMCs) for Aerospace Applications. Polymers 2021;13:201. https://doi.org/10.3390/polym13020201.

[6] Ghazali H, Ye L, Zhang MQ. Mode II interlaminar fracture toughness of CF/EP composite containing microencapsulated healing resins. Compos Sci Technol 2017;142:275–85. https://doi.org/10.1016/j.compscitech.2017.02.018.
[7] Baniasadi M, Yarali E, Bodaghi M, Zolfagharian A, Baghani M. Constitutive Modeling of multi-stimuli-responsive shape memory polymers with multi-functional capabilities. Int J Mech Sci 2021;192:106082. https://doi.org/10.1016/j.ijmecsci.2020.106082.
[8] Jony B, Roy S, Mulani SB. Fracture resistance of in-situ healed CFRP composite using thermoplastic healants. Mater Today Commun 2020;24:101067. https://doi.org/10.1016/j.mtcomm.2020.101067.
[9] Jony B, Vishe NJ, Roy S. Thermoplastic self-healing of mode I and mode II quasi-static and fatigue crack growth in CFRP composite using PCL/SMP dual phase healant, 2019. https://doi.org/10.12783/asc34/31403.
[10] Grande AM, Martin R, Odriozola I, van der Zwaag S, Garcia SJ. Effect of the polymer structure on the viscoelastic and interfacial healing behaviour of poly(urea-urethane) networks containing aromatic disulphides. Eur Polym J 2017;97:120–8. https://doi.org/10.1016/j.eurpolymj.2017.10.007.
[11] Aguirre De Cárcer I, Prolongo MG, Salom C, Parrado J, Moriche R, Prolongo SG. Thermal and mechanical properties of self-healing epoxy/graphene nanocomposites. vol. 2017- January, 2017, p. 1399–408.
[12] Zadeh MA, Grande AM, Zwaag S van der, Garcia SJ. Effect of curing on the mechanical and healing behaviour of a hybrid dual network: a time resolved evaluation. RSC Adv 2016;6:91806–14. https://doi.org/10.1039/C6RA17799A.
[13] Zhang L, Tian X, Malakooti MH, Sodano HA. Novel self-healing CFRP composites with high glass transition temperatures. Compos Sci Technol 2018;168:96–103. https://doi.org/10.1016/j.compscitech.2018.09.008.
[14] Post W, Cohades A, Michaud V, van der Zwaag S, Garcia SJ. Healing of a glass fibre reinforced composite with a disulphide containing organic-inorganic epoxy matrix. Compos Sci Technol 2017;152:85–93. https://doi.org/10.1016/j.compscitech.2017.09.017.
[15] Kostopoulos V, Kotrotsos A, Tsantzalis S, Tsokanas P, Christopoulos AC, Loutas T. Toughening and healing of continuous fibre reinforced composites with bis-maleimide based pre-pregs. Smart Mater Struct 2016;25:084011. https://doi.org/10.1088/0964-1726/25/8/084011.
[16] Pérez-Galmés M, Renart J, Sarrado C, Brunner AJ, Rodríguez-Bellido A. Towards a consensus on mode II adhesive fracture testing: Experimental study. Theor Appl Fract Mech 2018;98:210–9. https://doi.org/10.1016/j.tafmec.2018.09.014.
[17] Oliveira BMA de, Campilho RDSG, Silva FJG, Rocha RJB. Comparison between the ENF and 4ENF fracture characterization tests to evaluate GIIC of bonded aluminium joints. J Adhes 2018;94:910–31. https://doi.org/10.1080/00218464.2017.1387056.
[18] Wang W-X, Nakata M, Takao Y, Matsubara T. Experimental investigation on test methods for mode II interlaminar fracture testing of carbon fiber reinforced composites. Compos Part Appl Sci Manuf 2009;40:1447–55. https://doi.org/10.1016/j.compositesa.2009.04.029.
[19] Heo Y, Sodano HA. Thermally responsive self-healing composites with continuous carbon fiber reinforcement. Compos Sci Technol 2015;118:244–50. https://doi.org/10.1016/j.compscitech.2015.08.015.
[20] Singh T, Sehgal S. Structural Health Monitoring of Composite Materials. Arch Comput Methods Eng 2021. https://doi.org/10.1007/s11831-021-09666-8.
[21] Matveenko V, Serovaev G, Tashkinov M. Numerical Analysis of Delamination in Composite Structures Using Strain Measurements from Fiber Bragg Gratings Sensors, 2019, p. 62–7. https://doi.org/10.1007/978-3-319-91989-8_11.
[22] Bettini P, Airoldi A, Bogotto P, Loutas T. Interlaminar damage detection in composite elements by means of optical fibre sensors. vol. 2, 2017, p. 1172–85.
[23] Campanella CE, Cuccovillo A, Campanella C, Yurt A, Passaro VMN. Fibre Bragg Grating Based Strain Sensors: Review of Technology and Applications. Sensors 2018;18. https://doi.org/10.3390/s18093115.
[24] Canal LP, Sarfaraz R, Violakis G, Botsis J, Michaud V, Limberger HG. Monitoring strain gradients in adhesive composite joints by embedded fiber Bragg grating sensors. Compos Struct 2014;112:241–7. https://doi.org/10.1016/j.compstruct.2014.02.014.
[25] Farmand-Ashtiani E, Cugnoni J, Botsis J. Effects of large scale bridging in load controlled fatigue delamination of unidirectional carbon-epoxy specimens. Compos Sci Technol 2016;137:52–9. https://doi.org/10.1016/j.compscitech.2016.10.022.
[26] Kim H-S, Yoo S-H, Chang S-H. In situ monitoring of the strain evolution and curing reaction of composite laminates to reduce the thermal residual stress using FBG sensor and dielectrometry. Compos Part B Eng 2013;44:446–52. https://doi.org/10.1016/j.compositesb.2012.04.021.
[27] Luzuriaga AR de, Martin R, Markaide N, Rekondo A, Cabañero G, Rodríguez J, et al. Epoxy resin with exchangeable disulfide crosslinks to obtain reprocessable, repairable and recyclable fiber-reinforced thermoset composites. Mater Horiz 2016;3:241–7. https://doi.org/10.1039/C6MH00029K.
[28] Azcune I, Huegun A, Ruiz de Luzuriaga A, Saiz E, Rekondo A. The effect of matrix on shape properties of aromatic disulfide based epoxy vitrimers. Eur Polym J 2021;148:110362. https://doi.org/10.1016/j.eurpolymj.2021.110362.

[29] Zabala H, Aretxabaleta L, Castillo G, Aurrekoetxea J. Dynamic 4 ENF test for a strain rate dependent mode II interlaminar fracture toughness characterization of unidirectional carbon fibre epoxy composites. Polym Test 2016;55:212–8. https://doi.org/10.1016/j.polymertesting.2016.09.001.
[30] Ji F, Liu X, Sheng D, Yang Y. Epoxy-vitrimer composites based on exchangeable aromatic disulfide bonds: Reprocessibility, adhesive, multi-shape memory effect. Polymer 2020;197:122514. https://doi.org/10.1016/j.polymer.2020.122514.
[31] Chen J, Huang H, Fan J, Wang Y, Yu J, Zhu J, et al. Vitrimer Chemistry Assisted Fabrication of Aligned, Healable, and Recyclable Graphene/Epoxy Composites. Front Chem 2019;7.
[32] Benazzo F, Sodano HA. Evaluation of Interfacial Shear Strength Healing Efficiency between Dynamic Covalent Bond-Based Epoxy and Functionalized Fiberglass. ACS Appl Polym Mater 2022:4:2925–2934.
[33] Lima R de AA, Rocca D, Da Costa HRM, de Sousa JPB, Bettini P, Sala G, et al. Interfacial adhesion between embedded fibre optic sensors and epoxy matrix in composites. J Adhes Sci Technol 2019;33:253–72. https://doi.org/10.1080/01694243.2018.1537053.
[34] Kuang KSC, Kenny R, Whelan MP, Cantwell WJ, Chalker PR. Embedded fibre Bragg grating sensors in advanced composite materials. Compos Sci Technol 2001;61:1379–87. https://doi.org/10.1016/S0266-3538(01)00037-9.
[35] Fallais DJM, Henkel M, Noppe N, Weijtjens W, Devriendt C. Multilevel RTN Removal Tools for Dynamic FBG Strain Measurements Corrupted by Peak-Splitting Artefacts. Sensors 2022;22:92. https://doi.org/10.3390/s22010092.
[36] Matxain JM, Asua JM, Ruipérez F. Design of new disulfide-based organic compounds for the improvement of self-healing materials. Phys Chem Chem Phys 2016;18:1758–70. https://doi.org/10.1039/C5CP06660C.
[37] Shindo Y, Sato T, Narita F, Sanada K. Mode II Interlaminar Fracture and Damage Evaluation of GFRP Woven Laminates at Cryogenic Temperatures using the 4ENF Specimen. J Compos Mater 2008;42:1089–101. https://doi.org/10.1177/0021998308090451.
[38] Zile E, Tamuzs V. Mode II Delamination of a Unidirectional Carbon Fiber/Epoxy Composite in Four-Point Bend End-Notched Flexure Tests. Mech Compos Mater 2005;41:383–90. https://doi.org/10.1007/s11029-005-0064-2.
[39] Arrese A, Mujika F. Influence of bending rotations on three and four-point bend end notched flexure tests. Eng Fract Mech 2008;75:4234–46. https://doi.org/10.1016/j.engfracmech.2008.03.012.
[40] Khan R. Fiber bridging in composite laminates: A literature review. Compos Struct 2019;229:111418. https://doi.org/10.1016/j.compstruct.2019.111418.